Environ. Sci. Technol. **2007**, *41,* 5548−5558

Revisiting the Cape Cod Bacteria Injection Experiment Using a Stochastic Modeling Approach

REED M. MAXWELL,*,† CLAIRE WELTY,‡ AND RONALD W. HARVEY§

Atmospheric, Earth, and Energy Sciences Department, Lawrence Livermore National Laboratory (L-208), 7000 East Avenue, Livermore, California 94550, University of Maryland Baltimore County, Department of Civil and Environmental Engineering and Center for Urban Environmental Research and Education, 1000 Hilltop Circle, TRC 102, Baltimore, Maryland 21250, U.S. Geological Survey, 3215 Marine St., Ste. E-127, Boulder, Colorado 80303

Bromide and resting-cell bacteria tracer tests conducted in a sandy aquifer at the U.S. Geological Survey Cape Cod site in 1987 were reinterpreted using a three-dimensional stochastic approach. Bacteria transport was coupled to colloid filtration theory through functional dependence of local-scale colloid transport parameters upon hydraulic conductivity and seepage velocity in a stochastic advection−dispersion/attachment−detachment model. Geostatistical information on the hydraulic conductivity (K) field that was unavailable at the time of the original test was utilized as input. Using geostatistical parameters, a groundwater flow and particle-tracking model of conservative solute transport was calibrated to the bromide-tracer breakthrough data. An optimization routine was employed over 100 realizations to adjust the mean and variance of the natural-logarithm of hydraulic conductivity (ln*K*) field to achieve best fit of a simulated, average bromide breakthrough curve. A stochastic particle-tracking model for the bacteria was run without adjustments to the local-scale colloid transport parameters. Good predictions of mean bacteria breakthrough were achieved using several approaches for modeling components of the system. Simulations incorporating the recent Tufenkji and Elimelech (*Environ. Sci. Technol.* **2004**, *38*, 529−536) correlation equation for estimating single collector efficiency were compared to those using the older Rajagopalan and Tien (*AIChE J.* **1976**, *22*, 523−533) model. Both appeared to work equally well at predicting mean bacteria breakthrough using a constant mean bacteria diameter for this set of field conditions. Simulations using a distribution of bacterial cell diameters available from original field notes yielded a slight improvement in the model and data agreement compared to simulations using an average bacterial diameter. The stochastic approach based on estimates of local-scale parameters for the bacteria-transport process reasonably captured the mean bacteria transport behavior and calculated an envelope of uncertainty that bracketed the observations in most simulation cases.

1. Introduction

Ongoing reports of waterborne disease outbreaks (*3*) and the presence of pathogens in groundwater (e.g., refs *4*−*10*) underscore the need for advancement in our ability to predict subsurface pathogen transport. Such quantification is necessary for risk assessment and for development of pathogen total maximum daily loads (TMDLs) (*11*). Implementation of mechanistic mathematical models is one approach, but application is complicated by site-specific geologic heterogeneity and uncertainties, including parametrization of nonideal microbial transport properties in aquifer materials. Over the past 25 years, controlled laboratory studies involving homogeneous media have resulted in significant progress toward quantifying the roles of microbial (size, shape, surface chemistry), mineral, and fluid properties on the transport of microorganisms through the terrestrial subsurface (see ref *12* and reviews in refs *13* and *14*). Gains have also been made in the area of field-scale modeling by coupling porous-media transport models with a realistic representation of the microbial attachment process (e.g., refs *15* and *16*). Less progress has been made in coupling the known nonidealities of microbial transport with a realistic representation of aquifer heterogeneity to quantify the effects of heterogeneity on the transport process (e.g., refs *17*−*21*). However, the latter type of work is needed to produce models that better capture the field-scale reality of this complex process.

Since earlier attempts to couple colloid filtration with the advection−dispersion equation to model the movement of indigenous, uncultured bacteria in a controlled field-scale tracer tests (e.g., ref *15*), considerable advances have been made in (1) statistically quantifying physical aquifer heterogeneity; (2) capturing heterogeneity using numerical methods incorporating finely gridded systems and grid-free transport algorithms; (3) refining the relationship between colloid filtration (sorptive removal) and physical heterogeneity, and (4) parametrizing the colloid filtration process. The purpose of this paper is to utilize improvements in these four areas to revisit the data interpretation from the 1991 paper by Harvey and Garabedian. We make use of information from a site-specific geostatistical characterization of physical heterogeneity (hydraulic conductivity), particle-tracking numerical techniques that facilitate modeling on a fine grid and incorporation of input bacterial cell-size distributions, and postulated correlations (Rehmann et al. (*17*)) between colloid filtration and ln*K*. We also utilize recent improvements in estimations of the collector efficiency parameter in colloid filtration by Tufenkji and Elimelech (*1*), as compared to the more commonly used Rajagopalan and Tien (*2*) model. This paper evaluates how these improvements affect data interpretation and highlights areas where further work is needed.

2. Materials and Methods

2.1. Field Experiment. In October 1987, a short-scale (6.8 m) natural-gradient injection test involving indigenous bacteria fluorescently labeled with the fluorochrome 4,6-diamidino-2-phenylindole (DAPI) was conducted in the sandy aquifer at the U.S. Geological Survey Toxic Substances Hydrology research site at Cape Cod, Massachusetts. Details of the conditions of the injection test are provided in Harvey and

* Corresponding author phone: (925) 422-7436; fax: (925) 422-3925; e-mail: maxwell5@llnl.gov.
† Lawrence Livermore National Laboratory.
‡ University of Maryland Baltimore County.
§ U.S. Geological Survey.

10.1021/es062693a CCC: $37.00

Published on Web 06/30/2007

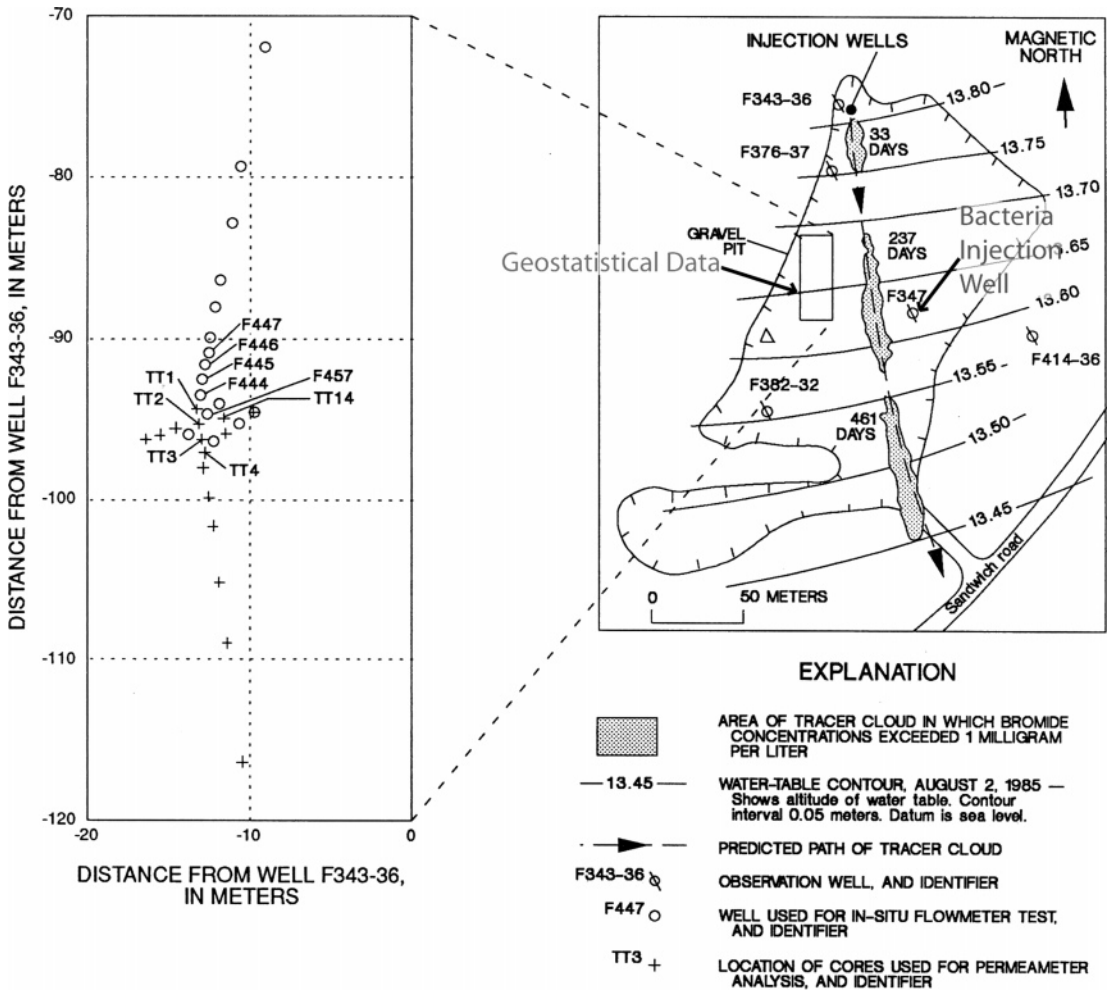

FIGURE 1. Location of the 1987 bacteria injection test (*15*) in relation to the sample plot where characterization of the geostatistical distribution of aquifer properties (*23*) was carried out and to the trajectory of the bromide cloud created during an earlier large-scale conservative tracer study (*22*). This figure adapted from Hess et al. (ref *23*) is reprinted with permission of American Geophysical Union.

Garabedian (*15*); information on the site hydrogeology is provided in LeBlanc et al. (*22*). In brief, a 90 L volume of bromide solution (150 mg/L) and stained bacteria was injected at a rate of 0.85 L/m simultaneously at depths of 8.5 and 9.1 m below land surface in the saturated zone. Breakthrough was subsequently measured for the aforementioned depths at 6.8 m downgradient from point of injection. At about the same time the tracer test was being conducted, an extensive characterization of the nature and distribution of the hydraulic conductivity properties of aquifer sediments was being carried out at a nearby plot by means of borehole flow meter measurements (*23*). The location of the two tests relative to one another is shown in plan view Figure 1. The vertical position of the injection points relative to the vertical depth over which the aquifer geostatistical information was obtained is shown in Figure 2.

Two additional data sets that were recorded during the 1987 tracer test, but not previously reported, include (1) breakthrough observations at two elevations at multilevel sampler M7, 5 m downgradient and about 1 m east of the centerline between the injection point and observation well M1, and (2) the histogram of the distribution of the sizes of the injected bacteria (Figure 3).

2.2. Governing Equations. The governing equation for local-scale advection, dispersion, and reversible interactions with grain surfaces for resting-cell bacteria in porous media is given by

$$\frac{\partial C_j}{\partial t} + \nabla\cdot(\boldsymbol{v}C_j) - \nabla\cdot(\boldsymbol{D}\cdot\nabla C_j) = -k_j^{att}C_j + k_j^{det}\frac{\rho_b}{\rho n}S_j \quad (1)$$

For attached bacteria, the mass balance equation is given by

$$\frac{\rho_b}{\rho n}\frac{\partial S_j}{\partial t} = k_j^{att}C_j - k_j^{det}\frac{\rho_b}{\rho n}S_j \quad (2)$$

where C_j is the mass fraction (dimensionless) of bacteria in solution of species or attribute j, S_j is the mass fraction (dimensionless) of attached bacteria of attribute j, k_j^{att} and k_j^{det} are first-order rate constants for physical/chemical attachment (sorption) and detachment of species j, ρ and ρ_b are densities of the fluid and bulk porous medium [M/L^3], $\boldsymbol{D}$ is the hydrodynamic dispersion tensor [L^2/T], $\boldsymbol{v}$ is the average seepage velocity [L/t], and n is effective porosity (dimensionless). Growth and death terms are not included in eqs 1 and 2 because abundances of DAPI-stained bacteria in a control suspension and in tracer test samples were stable during a 30-day period following collection (*15*). Although significant advances have been made in understanding the effect of bacterial chemotaxis at the pore scale (*24*), much about the macroscale significance of chemotaxis for bacteria is still poorly understood (*25*). However, DAPI, which is known

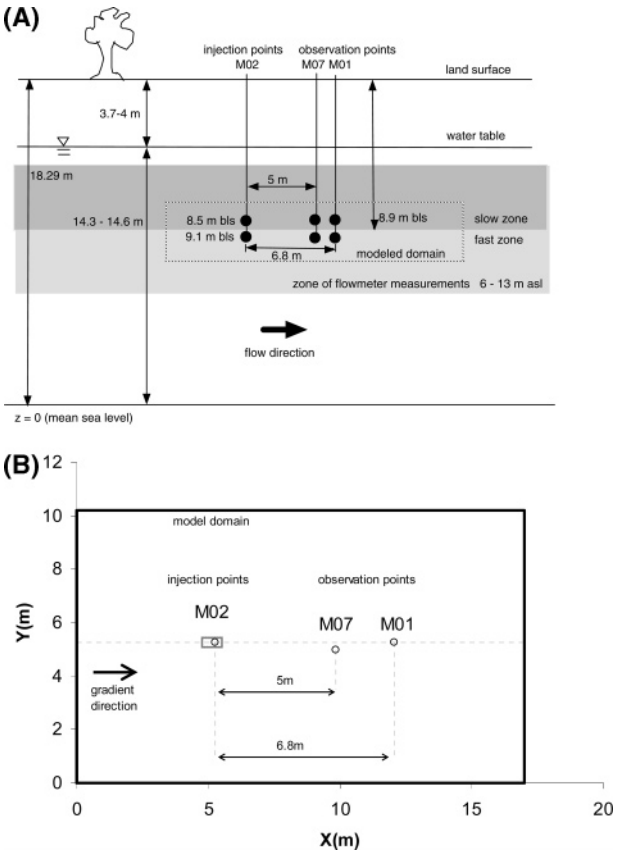

FIGURE 2. (a) Location of injection and observation points for tracer test. Vertical extent of nearby (*23*) flowmeter measurements used to calculate hydraulic conductivity is shown in gray. Fast and slow zones described by Harvey and Garabedian (*15*) are depicted. (b) Plan view of model domain with injection and observation wells identified. Note that Well M07 is located 0.31 m off-axis from Wells M02, M02 and the hydraulic gradient.

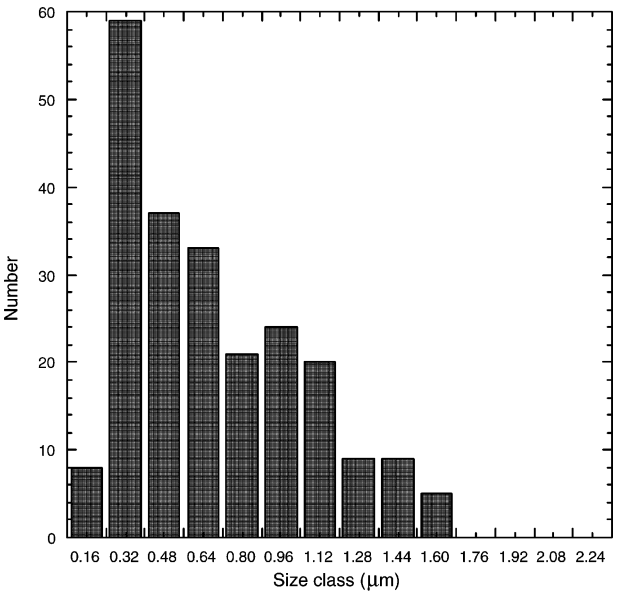

FIGURE 3. Distribution of diameters of indigenous bacteria injected in the 1987 tracer test.

to hamper bacterial activity (*26*), has recently been shown to inhibit chemotactic activity in groundwater bacteria (*27*). Also, the uncultured bacteria were stored in nutrient-depleted water prior to injection to lessen the formation of temporal gradients in dissolved organic carbon. Consequently, the effects of chemotaxis are assumed to be minor and, therefore, are not included in eqs 1 and 2.

Parametrization of k_j^{att} for subsurface microbial transport in aquifers using colloid filtration theory developed for ideal porous media was first proposed by Harvey and Garabedian (*15*) and has been utilized by a number of other researchers (e.g., Rehmann et al., (*17*); Schijven et al. (*16*)). This model is popular because it is based on fundamental thermodynamic principles, and because most of its parameters are published constants or can be measured. A widely used model for colloid filtration is that of Rajagopalan and Tien (R&T) (*2*), as modified by Martin et al. (*28*) and clarified by Logan et al. (*29*), which is given as

$$k_j^{att} = \left[\frac{3}{2}\frac{(1-n)}{d_{10}}\alpha_c\eta\right]v \quad (3)$$

where v is the groundwater velocity magnitude [L/T], η is the collision frequency, or single collector efficiency (dimensionless), α_c is the collision efficiency factor, or probability that collision will result in attachment (dimensionless) and d_{10} is the sieve size [m] for which 90% of grains of the porous medium are retained. The d_{10} is used as the representative grain diameter in heterogeneous media, based on the work of Martin et al. (*28*).

R&T estimated the collision frequency to be composed of additive factors influenced by Brownian motion, interception of the colloids by grains, and gravitational settling:

$$\eta = 4A_s^{1/3}N_{Pe}^{-2/3} + A_s N_{Lo}^{1/8} N_R^{15/8} + 0.00338 A_s N_G^{1.2} N_R^{-0.4} \quad (4)$$

where

$$A_s = \frac{2[1-(1-n)^{5/3}]}{[2-3(1-n)^{1/3}+3(1-n)^{5/3}-2(1-n)^2]}$$

$$N_R = \frac{d_p}{d_{10}}$$

$$D_p = \frac{B_z T}{3\pi\mu d_p}$$

$$N_{Pe} = \frac{nvd}{D_p} = \frac{3\pi\mu}{B_z T} nvd_{10}d_p$$

$$N_{Lo} = \frac{4H}{9\pi\mu d_p^2 v_p}$$

$$N_G = \frac{2}{9}\frac{d_p^2(\rho_p-\rho)g}{4\mu vn} = \frac{d_p^2(\rho_p-\rho)g}{18\mu vn}$$

and H is the Hamaker constant [M/L^{2}T^2], B_z is the Boltzmann constant [M/L^{2}T^2°K], T is temperature (°K), μ is dynamic viscosity [M/LT], d_p is colloid diameter [L], ρ is the fluid density [M/L^3], and ρ_p, the buoyant density of the colloidal particle [M/L^3]. A recent alternative formulation of collision frequency has been proposed by Tufenkji and Elimelech (T&E) (*1*), which the authors have shown to have an improved fit to lab data compared to the R&T model:

$$\eta = 2.4A_s^{1/3}N_R^{-0.081}N_{Pe}^{-0.715}N_{vdW}^{0.052} + 0.55A_s N_R^{1.675}N_A^{0.125} + 0.22N_R^{-0.24}N_G^{1.11}N_{vdW}^{0.053} \quad (5)$$

TABLE 1. Input Data for Particle Simulations

parameter	value	reference
ρ_b	1720 kg/m^3	Harvey and Garabedian (*15*)
r	999 kg/m^3	Harvey and Garabedian (*15*)
ρ_p	1010 kg/m^3	Harvey et al. (*55*)
n	0.39	LeBlanc et al. (*22*)
H	3×10^{-21} kg m^2/s^2	Tufenkji and Elimelech (*1*)
B_z	1.38×10^{-23} kg-m^2/s^{2}K	
T	288 °K	Harvey and Garabedian (*15*)
μ	1.14×10^{-3} kg/m-sec	Harvey and Garabedian (*15*)
d_p (average)	6.0×10^{-7} m	Harvey and Garabedian (*15*)
J (hydraulic gradient)	0.0015	LeBlanc et al. (*22*)
$\bar{K}$ at 9.1 m BLS[1]	78 m/d	calculated from reported *v*, *n*, assumed *J*
$\bar{K}$ (fast zone) at 8.5 m BLS[a]	77 m/d	calculated from reported *v*, *n*, assumed *J*
$\bar{K}$ (slow zone) at 8.5 m BLS[a]	58 m/d	calculated from reported *v*, *n*, assumed *J*
α_L, α_T	0.0 m	taken as zero in simulations, since effect of finite value was not discernible via test runs.
a_3	3.4×10^{-10}	from exponential fit to local-scale α_c $-\ln K$ data (Figure 4)
b_3	2.1	from exponential fit to local-scale α_c $-\ln K$ data (Figure 4)
δ_3	0	
a_2	9.46 10^{-7} sec^{-1}	from linear regression of detachment data in Schijven et al. (*16*)
b_2	1.03 10^{-7} sec^{-1}	from linear regression of detachment data in Schijven et al. (*16*)
δ_2	0	
$\sigma^2_{\ln K}$	0.24	Hess et al. (*23*)
$\lambda_{x,y}$	3.6 m	Hess et al. (*23*)
λ_z	0.19 m	Hess et al. (*23*)

[a] This parameter is used to assign initial values in parameter estimation procedure.

where

$$N_{vdW} = \frac{H}{B_z T}$$

$$N_A = \frac{N_{vdW}}{N_R N_{Pe}} = \frac{4H}{12\pi\mu d_p^2 vn} = \frac{H}{3\pi\mu d_p^2 vn}$$

Physical interpretations of the dimensionless parameters in eqs 4 and 5 can be found in Table 1 of Tufenkji and Elimelech (*1*).

2.3. Effect of Hydraulic Conductivity Variability on Microbial Transport. Hess et al. (*23*) have shown that the three-dimensional distribution of the natural-logarithm of hydraulic conductivity (ln*K*) of the aquifer material at the Cape Cod site can be represented as a stationary, correlated random field on the scale of tens of meters. Of interest is how this spatial variability in ln*K* couples with and affects the colloid transport process as represented by eqs 1 and *2*. It is well-known that ln*K* affects the fluid velocity (v) directly through Darcy's law. For the colloidal transport case, there is additional nonlinear dependence on ln*K* through the expression for attachment. From eq *3* it can be seen that

$$k_j^{att} = f(v, \ln K) \tag{6}$$

Dependence on v is direct as well as through the expression for $\eta(v)$ given by eqs 4 or *5*. k_j^{att} is also dependent on ln*K* in η through known correlations between d_{10} and ln*K*, and through postulated relationships between α_c and ln*K*. To obtain a d_{10}-ln*K* relationship, we inverted the Hazen (*30*) formula

$$d_{10} = [10^{-4}\exp(\ln K)]^{0.5} \tag{7}$$

where K and d_{10} are in m/sec and m, respectively. Good agreement has been shown between local-scale K calculated using the Hazen formula from grain-size analysis and K measured on the same sample using a constant-head permeameter (*31*), for the Cape Cod data.

Correlations of the transport parameters α_c, and k_j^{det} with ln*K* have been postulated by Rehmann et al. (*17*) to be

$$\alpha_c = a_1 + b_1 \ln K + \delta_1 \tag{8}$$

$$k_j^{det} = a_2 + b_2 \ln K + \delta_2 \tag{9}$$

where a_i and b_i are constants, and δ_i represents the random portions of α_c or k_j^{det} that are not correlated with ln*K* (*32*, *33*). The general forms specified by eqs 8 and 9 allow positive ($b_i > 0$), negative ($b_i < 0$), or zero ($b_i = 0$) correlation with the ln*K* field. The uncorrelated portion δ_i accounts for spatial variability in conditions not related to the hydraulic conductivity of the porous medium (e.g., solution chemistry). Numerical values for a_i, b_i, and δ_i must be determined experimentally. An example data set showing the correlation of α_c and ln*K* is given by Ren et al. (*34*).

To prevent α_c from going to zero for large values of ln*K*, we have found that an alternative formula for eq 8 specified as

$$\alpha_c = a_3 \exp(-b_3 \ln K) + \delta_3 \tag{10}$$

is computationally advantageous. Figure 4 shows both a linear fit (eq 8) and an exponential fit (eq 10) to data taken from Ren et al. (*34*) and Dong et al. (*35*) (as expanded upon in Mailloux et al. Figure 10c, ref *36*) covering a wide range of ln*K* values. Values for α_c greater than one resulting from very small values of ln*K* using these correlations were not allowed and instead set equal to one.

2.4. Numerical Solution Using a Particle Tracking Approach. A Lagrangian particle-tracking approach was used to simulate both bromide and bacterial transport. Particle-tracking methods have been widely applied in subsurface transport problems (e.g., refs *37*–*40*). This approach transforms transport eqs 1 and 2 into a set of discrete particles such that each particle represents a small portion of the total mass of solute. A modification to the particle-tracking approach for a conservative tracer was used to represent the attached bacterial phase and the attachment/detachment kinetics presented in Section 2.2. This modification represents

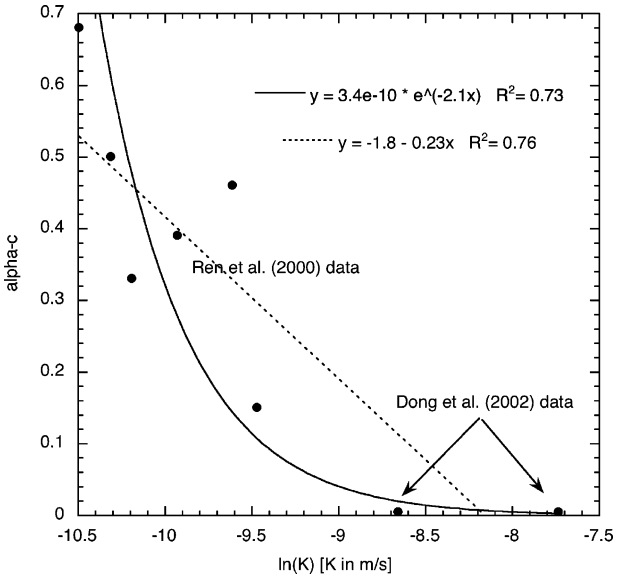

FIGURE 4. α_c vs ln*K* data from Ren et al. (2000) and Dong et al. (2002) (as supplemented by Mailloux et al. (ref *36*, Figure 10c) with linear and exponential fits to the data. The exponential fit was used in the model runs in this paper.

attachment and detachment rates as particle probability functions. For a given particle time step, an attachment or detachment probability is calculated and a random function is used to determine whether a given particle attaches to the soil matrix. This approach is similar to that introduced by Valocchi and Quinodoz (*41*) and used by Michalak and Kitanidis (*42*) for modeling kinetic chemical sorption, has been used to model matrix diffusion (e.g., Liu et al. (*43*)) and for microbial transport (Zhang et al. (*44*); Scheibe and Wood (*45*)). For large problems with heterogeneous physical parameters, this approach of representing attachment−detachment interactions as particle probabilities facilitates rapid solution of eqs 1 and 2 with mass conservation and no numerical dispersion. Also, each particle is moved according to a locally calculated, optimal time step, and may be split into two particles of equal mass if a single particle occupies a computational cell. These techniques further improve efficiency and accuracy, particularly for low concentrations (*46*) (please see the Supporting Information).

2.5. Generation of Hydraulic Conductivity Random Field. The two alluvial layers identified in Harvey and Garabedian (*15*) were conceptualized as having small-scale hydraulic conductivity (*K*) heterogeneity following a correlated, Gaussian random field, each with independent statistical parameters. The ln*K* variance ($\sigma^2_{\ln K}$) and correlation scales ($\lambda_x = \lambda_y$, λ_z) were taken as those reported by Hess et al. (*23*) from a nearby plot. Information reported by Harvey and Garabedian (*15*) was used to estimate initial values of the geometric mean *K* values for the two layers (Table 1). Using these statistical parameters, the small-scale variability in hydraulic conductivity of each layer was generated numerically using the turning bands approach of Tompson et al. (*47*). Because measurements made by Hess et al. (*23*) were not located directly in the Harvey and Garabedian (*15*) study plot, unconditional simulations were utilized.

Adjustment of the initial hydraulic conductivity field to obtain the best fit of simulated to measured (*14*) bromide transport was carried out as follows. A flow model, 17.0 m × 10.2 m × 3.8 m in the *x*, *y*, and *z* dimensions, respectively, was constructed with a 0.34 and 0.038 m lateral and vertical spatial discretization ($dx = dy$, dz), respectively, creating 50 × 30 × 100 finite difference cells (*nx*, *ny*, and *nz*). The finite-difference flow code ParFlow (*48*−*50*) was run for 100 realizations of the hydraulic conductivity field. The model was simulated as steady-state flow and constructed with constant head boundaries on the X_0 and X_{max} faces and "no-flow" conditions on all others to provide the observed gradient listed in Table 1. A bromide tracer was introduced as a pulse source of particles in a 0.765 m × 0.34 m × 1 m volume centered on M02 (6.8 m upgradient of M01) to achieve approximately the same injection conditions as the Harvey and Garabedian (*15*) field experiment. Figure 2 shows schematic details of the simulation domain. The average of the breakthrough curves generated by forward simulation over the 100 geostatistical realizations was compared to breakthrough field data for all four locations (wells M01 and M07, two upper, two lower). The parameter estimation code, PEST (*51*) was used to adjust the geometric mean *K* and ln*K* variance for the two layers using the difference between calculated average (over all 100 realizations) and observed bromide concentrations for all four monitoring locations as the objective function. The correlation scales were not adjusted. This process was run iteratively until the objective functions converged. At this point, a best fit to the bromide data was achieved and the ln*K* statistical parameters used to generate the optimal set of 100 realizations of the ln*K* field and the resulting 100 ln*K* realizations and flow fields were saved and used for the bacteria simulations. Table 2 provides the numerical parameters used in the flow and transport models.

TABLE 2. Input and Final Calibration Parameters for Flow and Particle Models

parameter	value	unit
dx	0.34	m
dy	0.34	m
dz	0.038	m
nx	50	
ny	30	
nz	100	
K_g_upper[a]	83	m/d
$\sigma_{\ln K}^2$_upper[a]	0.31	
K_g_lower[1]	87.5	m/d
$\sigma_{\ln K}^2$_lower[1]	0.22	
$\lambda_{x,y}$	3.60	m
λ_z	0.19	m
upper/lower domain split	8.91	m bls
domain size (*x*,*y*,*z*)	17.0 × 10.2 × 3.8	m
bottom of domain	10.41	m bls
upper zone thickness	2.3	m
lower zone thickness	1.5	m
number of initial particles	75 000	
maximum number of particles allowed after splitting	250 000	

[a] Final calibration values.

2.6. Bacteria Transport Simulations. Bacteria injection and downgradient transport was simulated using the flow fields resulting from the 100 hydraulic conductivity realizations generated by the bromide calibration. Bacteria transport was modeled using several options: (1) the R&T vs T&E formulations for attachment; (2) average vs particle size distribution for the bacteria sizes, and (3) constant vs variable detachment rates. This resulted in seven different bacterial transport cases, each of which was run over all 100 realizations of hydraulic conductivity. Although the community of unattached bacteria comprising the injectate included many rod-shaped cells, this model assumes uniform spherical morphology. In all bacterial transport runs, η was spatially variable, with grain diameter related to ln*K* (using the Hazen formula, eq 7), the velocity taken to be the magnitude of the local cell velocities, and α_c related to ln*K* using eq 10 as described in Section 2.3. This overall approach for relating filtration parameters to hydraulic conductivity is similar to

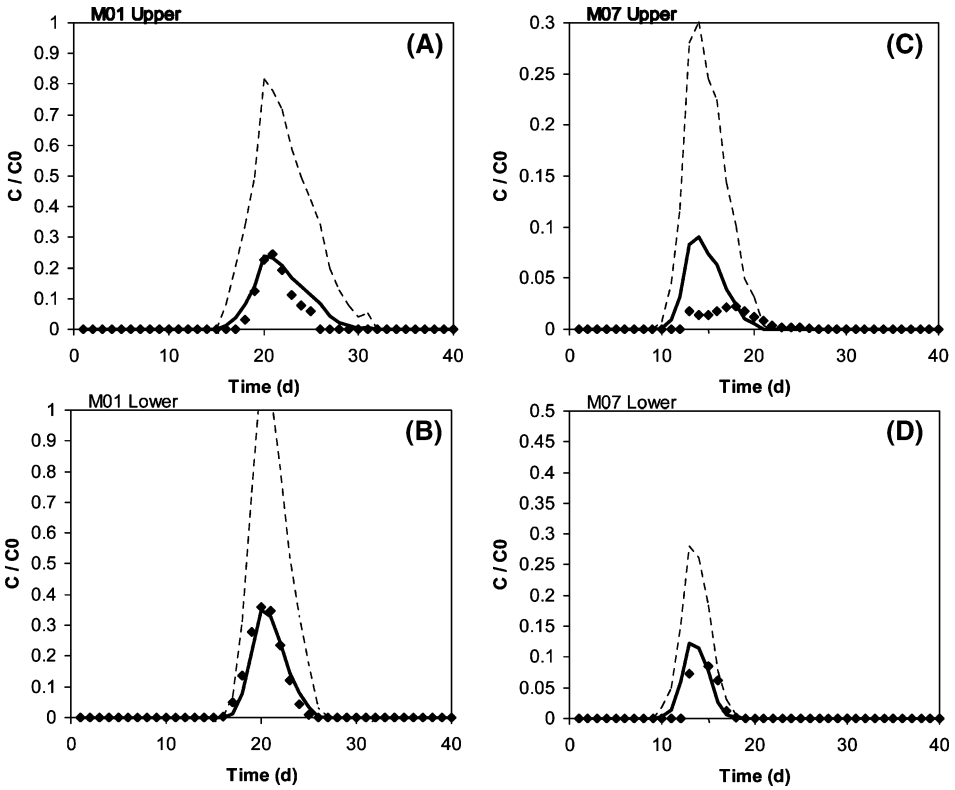

FIGURE 5. Plot of observed (symbols) and simulated (lines) bromide concentrations (normalized by initial concentration, C0) with time for both wells at both monitoring ports for the calibrated ensemble of realizations. Average simulated bromide plotted as a solid line with +1 standard deviation plotted as a dashed line.

that presented in Maxwell et al. (*20*). For each of the aforementioned seven cases, average bacteria breakthrough curves generated by simulation over the 100 geostatistical realizations were compared to field data for the upper and lower sampled ports of wells M01 and M07. Table 1 provides the physical input data used in the bacteria transport simulations. For all simulations, estimated values of local dispersivity (0.0005 m) had little effect compared to mixing due to heterogeneity, and therefore all runs were carried out with this parameter set equal to zero for computational efficiency.

3. Results

The results of the bromide calibration are given in Figure 5. The model results are depicted as the arithmetic mean over 100 realizations (heavy solid line) with the mean plus 1 standard deviation (over 100 realizations), plotted as a thin dashed line. The mean minus 1 standard deviation was zero for all tracer results. Table 2 lists the physical parameters that characterize the Gaussian random field resulting from the bromide calibration.

Plotted in Figure 6 are the observed and simulated bacterial transport concentrations at the upper and lower ports for well M01 and the lower port for well M07. During the original field experiment, bromide concentrations for the upper port of well M07 were very low and corresponding bacteria abundances could not be determined accurately because they were close to or below the detection limit. The corresponding model runs predicted very low bacterial concentrations (peak $C/C0 < 5 \times 10^{-3}$ for all simulations) and are therefore not plotted. The simulations in Figure 6 depict the attachment correlations parametrized using either the T&E expression (Figure 6a, b, c) or the R&T equation (Figure 6d, e, f) for an averaged bacterial size of 0.63 um. As for the bromide runs, the bacteria simulations are also plotted as the arithmetic mean (solid line) and ±1 standard deviation (dashed line) calculated over 100 realizations of the hydraulic conductivity random field. A constant detachment rate of $k_j^{det} = 0.02\ d^{-1}$ was used for all simulations.

Figure 7 shows the observed and simulated bacterial transport concentrations again use the T&E (Figure 7a, b, c) and R&T Figure 7d, e, f) expressions for bacterial attachment but instead of a constant bacteria diameter, the distribution of 10 bacteria diameters shown in Figure 3 was utilized. These simulations are also plotted as the arithmetic mean (solid line) and ±1 standard deviation (dashed line) calculated over 100 realizations of the hydraulic conductivity random field. Again a constant detachment rate of $k_j^{det} = 0.02\ d^{-1}$ was used for all simulations.

Figure 8 shows plots of simulations versus observations at all wells for the bromide and bacteria cases presented in Figures 5−7, with a linear regression through the data points and a 1:1 line (which would be a perfect fit) superimposed for comparison.

4. Discussion

4.1. Interpretation of Model Results. Figure 5 plots show a remarkably good agreement between observed and mean simulated peak bromide concentrations at the M01 upper and lower wells and the M07 lower well. Although simulation of peak bromide concentration at the M07 upper well is not as good as the three others—it is a factor of 4 higher than the observation—the simulated breakthrough curve does capture the approximately correct width of the observed bromide breakthrough at this location, and falls within the ±1 standard deviation of the mean simulation. This is most likely due to a local heterogeneous feature of the hydraulic conductivity present in the real system that is not captured by the model. For all wells other than M01 lower, the mean model first appearance of bromide precedes the observed data, indicating some error in the modeled ln$K$ field compared to the in-situ field. Nonetheless, the overall good agreement is borne

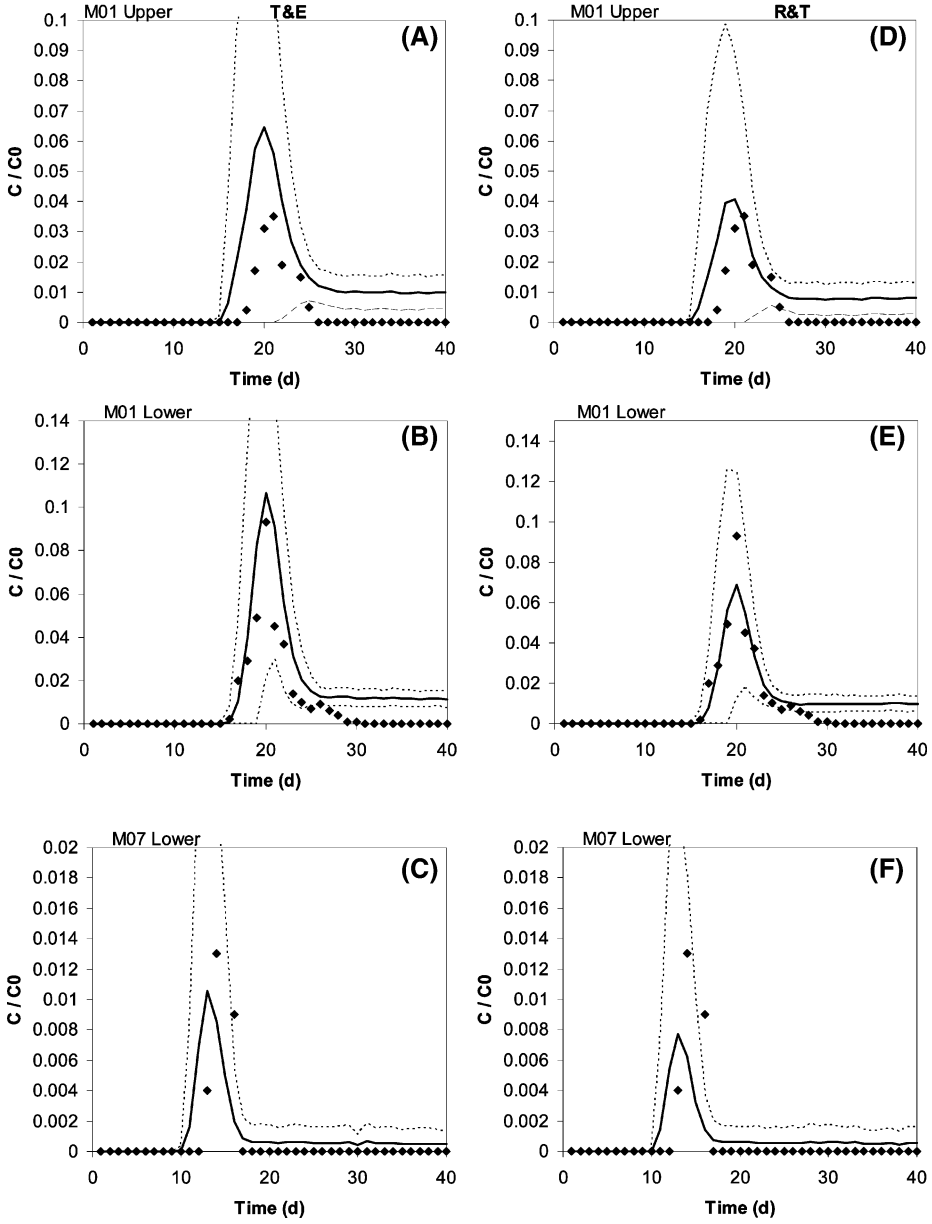

FIGURE 6. Plot of observed (symbols) and simulated (lines) bacterial concentrations (normalized by initial concentration, C0) with time (days) for sampling ports M01 upper, M01 lower, and M07 lower (expanded scale). The T&E (left, A−C) and R&T (right, D−F) attachment formulation are utilized with an averaged particle size. Average simulated bacterial concentrations plotted as a solid line with ± 1 standard deviation plotted as a dashed line.

out by the plot in Figure 8a, the slope of the best fit line through the observation versus simulation of all points at all wells is 0.96, with an R^2 of 0.88.

All of the simulated mean bromide concentrations fall within the envelope encompassed by ±1 model standard deviation. While this envelope may visually appear to be quite large for all wells, it should be recognized that this is due to the nature of the simulations, which were unconditional. However, if *K* data were available within the model domain on which the random fields could be conditioned, the standard deviation would be tighter. Given the overall good match of the simulated mean bromide to the breakthrough data, we have confidence that the heterogeneity of the test site is fairly well represented by the model results. We also point out that by using the numerical technique, where the heterogeneity is specified explicitly, we are not restricted from modeling transport over small distances, whereas this would be a problem using a small-perturbation stochastic analytical approach (e.g., ref *17*) necessitating transport over many correlation scales of a heterogeneous *K* field in order to satisfy ergodicity requirements.

Figure 6 shows the simulations of resting cell bacteria assuming a mean, constant bacteria diameter as input, for both the T&E and R&T models. All local-scale bacteria transport parameters were approximated from literature values. There was no parameter fitting involved and the same 100 ln*K* realizations and flow fields from the bromide calibrations were used. For all wells, simulated mean bacteria concentrations agree with the observations, and generally the observed data fall within ±1 standard deviation of the simulated mean. The simulated first arrival times of the bacteria at the M01 upper and M07 lower wells precede the observed first arrivals by several days, which is to be expected given the bromide results and bacteria detection limit limitations. Both the R&T and T&E colloid transport models appear to do an equal job using the constant bacteria diameter. This is confirmed by the plots in Figure 8b and c,

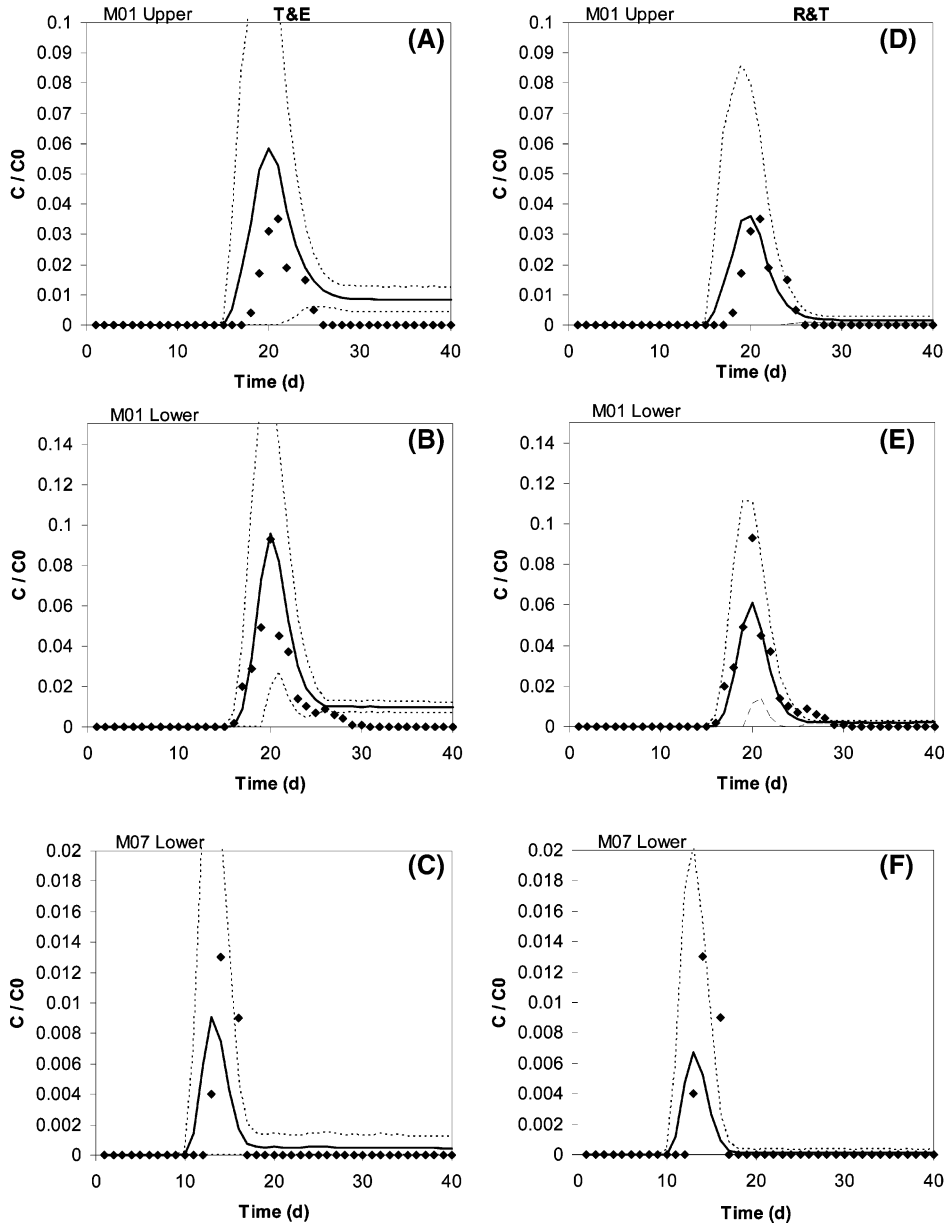

FIGURE 7. Plot of observed (symbols) and simulated (lines) bacterial concentrations (normalized by initial concentration, C0) with time for (days) sampling ports M01 upper, M01 lower, and M07 lower (expanded scale). The T&E (left, A−C) and R&T (right, D−F) attachment formulation are utilized with the particle size distribution given in Figure 3. Average simulated bacterial concentrations plotted as a solid line with ±1 standard deviation plotted as a dashed line.

the slopes of the linear regressions to the simulated versus observed data are 0.86 and 1.37 for the R&T and T&E cases, respectively, compared to a perfect fit of 1.0. Both models consistently overpredict the tailing behavior compared to the observations. Observed concentrations past 25 days do not fall within ±1 standard deviation of the simulated mean for well M01 upper or lower port.

Incorporation of the distribution of bacteria diameters in the numerical model, as illustrated by Figure 7, yields a slight improvement in model and data agreement, compared to Figure 6, most noticeably in the breakthrough after 25 days. In this case, the peak simulated breakthrough values of mean bacteria concentration are lower than for the constant-mean bacteria-diameter case and the widths of the breakthrough curves are also in better agreement. The slopes of the linear regressions in Figure 8 show about a 10% improvement for the T&E formulation (1.37 in Figure 8c compared to 1.24 in Figure 8e) while linear regression slopes do not change as much in the R&T formulation. The bacteria diameter affects the transport process in the expression for single collector efficiency (η), where the relative effects of diffusion, interception due to van der Waals forces, and gravity are incorporated into the local-scale expression as given by eqs 4 or 5. Figure 7 also indicates that incorporation of the new T&E model into the expression for local-scale single collector efficiency results in greater bacteria breakthrough than the R&T model. The overall difference in these two models corresponds to the lower single collector efficiency (η) for the bacterial size range predicted by the T&E formulation. This is also shown by Figure 8d and e, the slopes of the linear regression of the simulated versus observed data are 0.79 for the R&T and 1.24 for the T&E models. Figures 2 and 3 in Tufenkji and Elimelech (*1*) compare the single collector efficiencies calculated for a range of particle diameters for the R&T and T&E formulations. The range of particle diameters simulated in this current study corresponds to the region of largest difference between the two models.

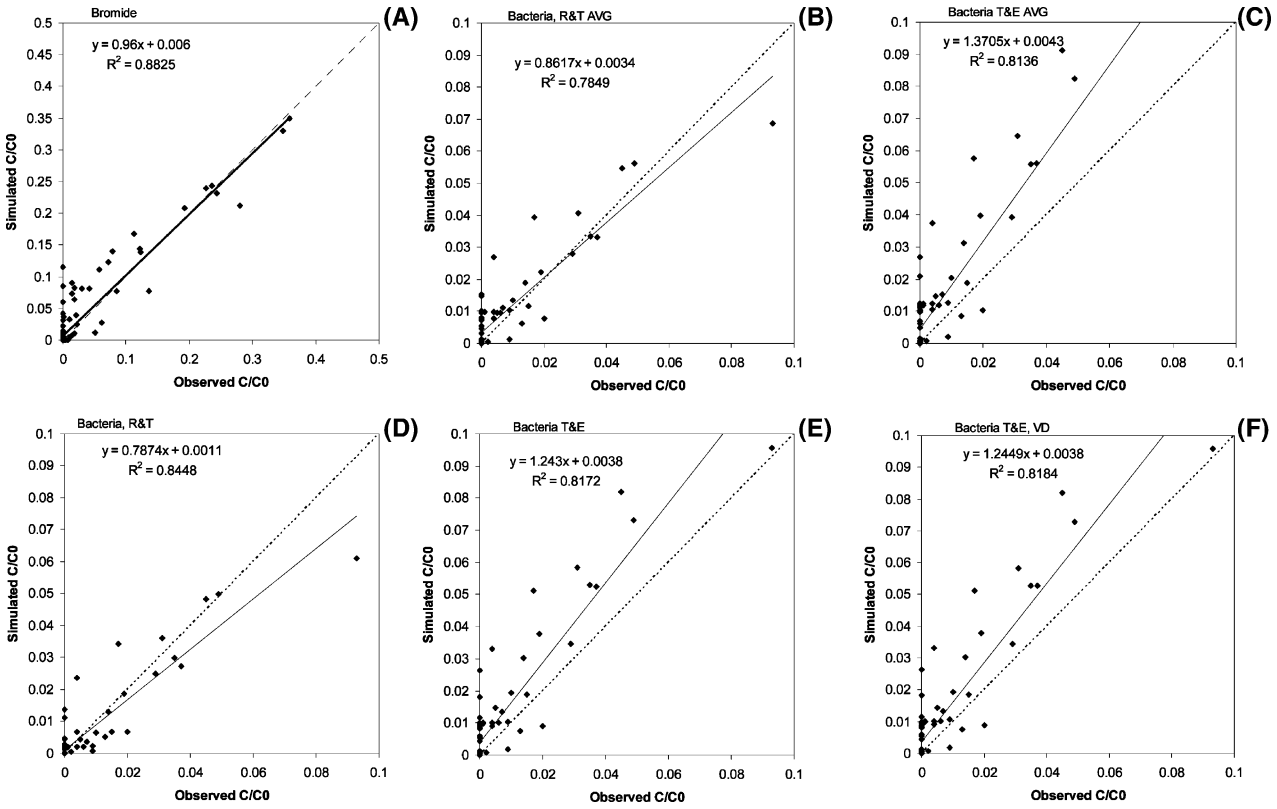

FIGURE 8. Plot of observed versus simulated averaged (arithmetic mean over all 100 realizations of hydraulic conductivity) concentrations for bromide and bacteria for all wells with 1 to 1 line (dotted) and linear fit noted on figure, for (a) bromide for all four monitoring locations; bacteria for the three nonzero monitoring locations for (b) constant diameter and R&T expression for η; (c) constant diameter with the T&E expression for η; (d) distribution of diameters and R&T expression for η; (e) distribution of diameters and T&E expression for η; and (f) distribution of diameters and T&E expression for η, with variable detachment.

Figures 6 and 7 show model results utilizing a constant detachment rate. The model was also run for the T&E case using a detachment rate correlated to hydraulic conductivity, thereby rendering a spatially variable detachment rate. These model runs show that spatial variability of detachment had little effect on breakthrough compared to the constant mean detachment case, i.e., the model results appear to be virtually identical to Figure 7 and, therefore, are not shown. Figure 8f shows the results of the simulated vs observed data for this case for all wells and it can be seen that it is virtually identical to Figure 8e. The tailing behavior of the breakthrough curves was not captured well either using a constant or spatially variable detachment rate; however, other factors not considered in this approach (e.g., chemical heterogeneity, discussed below) might contribute to this behavior.

4.2. Significance and Implications. We have reinterpreted breakthrough data for bromide and resting-cell bacteria injection tests conducted in 1987 and reported in 1991 (*15*) using computational tools and theoretical frameworks that were, for the most part, unavailable during the original study and analysis. The purpose of conducting the simulations and analysis of the data was to illustrate the applications of these advancements. This work may have implications for those intending to use the Harvey and Garabedian model in engineering applications (e.g., ref *52*).

Our analysis differs from that reported in 1991 in the following aspects. First, we utilized a fully three-dimensional transport model of the tracer tests, to better match the field conditions of the pulse injection in a three-dimensional flow field, whereas a one-dimensional analysis was previously employed. Second, we explicitly incorporated information on the physical heterogeneity of the hydraulic conductivity field as conditioned by information on observations of conservative tracer breakthrough. Use of the methods in this paper is, therefore, predicated upon information on the physical heterogeneity of the field site, i.e., the hydraulic conductivity distribution, being available. This can be an expensive undertaking and is still an active area of research in the field of hydrogeology (e.g. ref *53*, *54*). Although modeled as stationary (constant mean and variance), stationarity of the ln$K$ field is not required for the numerical methods used here. However, using approaches that rely on this assumption (e.g. ref *17*) could have limitations in other applications. This method is also not restricted in applications to near-field problems where it would be expected that macroscopic behavior may be non-Fickian at such scales. Also, we utilized unconditional simulations because K data were not available in the test plot on which to condition the simulations; availability of these data would have significantly reduced the standard deviation around the mean for the simulated breakthrough curves.

Third, we were successful at simulating bacteria transport using a stochastic numerical approach with no parameter fitting of the bacteria transport and filtration parameters. After calibrating 100 unconditional K random field realizations based on optimization of the mean and standard deviation of the ln$K$ field to provide a best fit of the bromide breakthrough curves, we were able to show good simulation of bacteria transport/filtration where local scale parameters are spatially variable. Prediction of bacteria breakthrough was improved in the T&E formulation by replacing averaged bacterial size with a full bacterial size distributions. The latter modification is easily incorporated using the particle-tracking approach because particles can be assigned variable properties such as diameter. Apparently, the dependence of the single collector efficiency on bacteria diameter is significant even for field applications because the sensitivity of the relative importance of diffusion, interception, and settling

on bacteria diameter (eqs 4 or 5).

Fourth, the stochastic framework utilized here, as postulated by Rehmann et al. (*17*), is dependent upon the assumption of correlation of the colloid filtration parameters and detachment with the spatial variability of hydraulic conductivity, and the availability of data to parametrize this correlation. However, such experimental data are scarce. This type of fairly site-specific correlation data can be generated by fairly simple laboratory experiments (see, e.g., ref *34*) and is needed for determining the range of correlation parameters physically feasible. As demonstrated by hypothetical simulations in Maxwell et al. (*20*), the model results are quite sensitive to values of the correlation parameters. Improvements can be made as published data become available on correlations between colloid transport parameters and ln$K$ for the sedimentary materials from this field site.

Acknowledgments

This material is based upon work supported by National Science Foundation Grant #no. BES-0226460 and partly by the U.S. Environmental Protection Agency under grants R-82818201-0 and CR83105801. Although the research described in this paper has been funded in part by the U.S. Environmental Protection Agency, it has not been subjected to the Agency's required peer and policy review and, therefore, does not necessarily reflect the views of the Agency and no official endorsement should be inferred. Portions of this work were conducted under the auspices of the U.S. Department of Energy by the University of California, Lawrence Livermore National Laboratory (LLNL) under contract W-7405-Eng. The installation of well site F347 used in the 1987 bacterial transport test and test data relating to bacterial size distributions and concentration histories were collected with financial assistance from the U.S.Geological Survey Toxic Substances Hydrology Program. We wish to thank J. Lawson of JHU for assistance in setting up a preliminary version of the numerical model used in this work.

Supporting Information Available

The particle tracking numerical model is described in detail. This material is available free of charge via the Internet at http://pubs.acs.org.

Literature Cited

(1) Tufenkji, N.; Elimelech, M. Correlation equation for predicting single-collector efficiency in physicochemical filtration in saturated porous media. *Environ. Sci. Technol.* **2004**, *38* (2), 529−536.

(2) Rajagopalan, R.; Tien, C. Trajectory analysis of deep-bed filtration with sphere-in-cell porous-media model. *AIChE J.* **1976**, *22* (3), 523−533.

(3) Blackburn, B.; Craun, G. F.; Yoder, J.; Hill, V.; Calderon, R. L.; Chen, N.; Lee, S. H.; Levy, D. A.; Beach, M. J. *Surveillance for Waterborne-Disease Outbreaks Associated with Drinking Water−United States, 2001−2002, Morbidity and Mortality Weekly Report*, October 22, 53(SS08); Centers for Disease Control and Prevention: Atlanta, GA, 2004; pp 23−45.

(4) Banks, W. S. L.; Klohe, C. A.; Battigelli, D. A. *Occurrence and Distribution of Enteric Viruses in Shallow Ground Water and Factors Affecting Well Vulnerability to Microbiological Contamination in Worcester and Wicomico Counties, MD*, Water Resources Investigations Report 01−4147; U.S. Geological Survey: Reston, VA, 2001.

(5) Lindsey, B. D.; Rasberry, J. S.; Zimmerman, T. M. *Microbiological Quality of Water from Noncommunity Supply Wells in Carbonate and Crystalline Aquifers of Pennsylvania*, Water-Resources Investigations Report 01−4268; U.S. Geological Survey: Reston, VA, 2002.

(6) Abbaszadegan, M.; Lechevallier, M.; Gerba, C. Occurrence of viruses in US groundwaters. *J. Am. Water Works Assoc.* **2003**, *95* (9), 107−120.

(7) Borchardt, M. A., Bertz, P. D.; Spencer, S. K.; Battigelli, D. A. Incidence of enteric viruses in groundwater from household wells in Wisconsin. *Appl. Environ. Microbiol.* **2003**, *69* (2), 1172−1180.

(8) Borchardt, M. A.; Haas, N. L.; Hunt, R. J. Vulnerability of drinking-water wells in La Crosse, Wisconsin, to enteric-virus contamination from surface water contributions. *Appl. Environ. Microbiol.* **2004**, *70* (10), 5937−5946.

(9) Powell, K. L.; Taylor, R. G.; Cronin, A. A.; Barrett, M. H.; Pedley, S.; Sellwood, J.; Trowsdale, S. A.; Lerner, D. N. Microbial contamination of two urban sandstone aquifers in the UK. *Water Res.* **2003**, *37* (2), 339−52.

(10) Francy, D. S.; Bushon, R. N.; Stoper, J.; Luzano, E.; Fout, G. S. *Environmental Factors and Chemical and Microbiological Water-Quality Constituents Related to the Presence of Enteric Viruses in Groundwater from Small Public Water Supplies in Southeastern Michigan*, Scientific Investigations Report 2004−5219; U.S. Geological Survey: Reston, VA, 2004; p 54 pp.

(11) Agency, U. S. E. P., *Protocol for Developing Pathogen TMDLs,* Office of Water (4503F); United States Environmental Protection Agency: Washington, DC, 2001; p 132.

(12) Keller, A. A.; Sirivithayapakorn, S.; Chrysikopoulos, C. V. Early breakthrough of colloids and bacteriophage MS2 in a water-saturated sand column. *Water Resour. Res.* **2004**, *40* (8), 1−11.

(13) Jin, Y.; Flury, M. *Fate and Transport of Viruses in Porous Media,* Advances in Agronomy; Elsevier Science Direct: New York, 2002; Vol. 77, p 39.

(14) Schijven, J. F.; Hassanizadeh, S. M. Removal of viruses by soil passage: Overview of modeling, processes, and parameters. *Crit. Rev. Environ. Sci. Technol.* **2000**, *30* (1), 49−127.

(15) Harvey, R. W.; Garabedian, S. P. Use of colloid filtration theory in modeling movement of bacteria through a contaminated sandy aquifer. *Environ. Sci. Technol.* **1991**, *25* (1), 178−185.

(16) Schijven, J. F., et al. Modeling removal of bacteriophages MS2 and PRD1 by dune recharge at Castricum, Netherlands. *Water Resour. Res.* **1999**, *35* (4), 1101−1111.

(17) Rehmann, L. L. C.; Welty, C.; Harvey, R. W. Stochastic analysis of virus transport in aquifers. *Water Resour. Res.* **1999**, *35* (7), 1987−2006.

(18) Sun, N., et al. A novel two-dimensional model for colloid transport in physically and geochemically heterogeneous porous media. *J. Contam. Hydrol.* **2001**, *49* (3−4), 173−199.

(19) Bhattacharjee, S.; Ryan, J. N.; Elimelech, M. Virus transport in physically and geochemically heterogeneous subsurface porous media. *J. Contam. Hydrol.* **2002**, *57* (3−4), 161−187.

(20) Maxwell, R. M.; Welty, C.; Tompson, A. F. B. Streamline-based simulation of virus transport resulting from long term artificial recharge in a heterogeneous aquifer. *Adv. Water Resour.* **2003**, *26* (10), 1075−1096.

(21) Scheibe, T. D.; Dong, H.; Xie, Y.-L. Correlation between bacterial attachment rate coefficients and hydraulic conductivity and its effect on field-scale bacterial transport. *Adv. Water Resour.* **2007**, *30* (6−7), 1571−1582.

(22) Leblanc, D. R.; Garabedian, S. P.; Hess, K. M.; Gelhar, L. W.; Quadri, R. D.; Stollenwerk, K. G.; Wood, W. W. Large-scale natural gradient tracer test in sand and gravel, Cape-Cod, Massachusetts. 1. Experimental design and observed tracer movement. *Water Resour. Res.* **1991**, *27* (5), 895−910.

(23) Hess, K. M.; Wolf, S. H.; Celia, M. A. Large-scale natural gradient tracer test in sand and gravel, Cape-Cod, Massachusetts. 3. Hydraulic conductivity variability and calculated macrodispersivities. *Water Resour. Res.* **1992**, *28* (8), 2011−2027.

(24) Barton, J. W.; Ford, R. M. Mathematical model for characterization of bacterial migration through sand cores. *Biotechnol. Bioeng.* **1997**, *53* (5), 487−496.

(25) Ford, R. M. a. R. W. H. Transport properties for motile and chemotactic bacteria in saturated porous media. *Adv. Water Resour.* **2007**, *30*, 1608−1617.

(26) Parolin, C., et al., The effect of the minor groove binding agent DAPI (4,6-diamidino-2-phenyl-indole) on DNA-directed enzymes: An attempt to explain inhibition of plasmid expression in Escherichia coli [corrected]. *FEMS Microbiol. Lett.* **1990**, *56* (3), 341−6.

(27) Toepfer, J. A. *The Impact of the Nucleic Acid Stain DAPI on the Motility and Chemotactic Behavior of the Soil-Dwelling Bacteria Pseudomonas putida F1*; Department of Chemical Engineering, University of Virginia: Charlottesville, VA, 2006.

(28) Martin, M. J.; Logan, B. E.; Johnson, W. P.; Jewett, D. G.; Arnold, R. G. Scaling bacterial filtration rates in different sized porous media. *J. Environ. Eng. Div. Am. Soc. Civ. Eng.* **1996**, *122* (5), 407−415.

(29) Logan, B. E.; Jewett, D. G.; Arnold, R. G.; Bouwer, E. J.; O'Melia, C. R. Clarification of Clean-Bed Filtration Models. *J. Environ. Eng. Div. Am. Soc. Civ. Eng.* **1995**, *121* (12), 869−873.

(30) Hazen, A. A discussion of "Dams on sand foundations" by A. C. Koenig. *Trans. Am. Soc. Civ. Eng.* **1911**, 73.

(31) Wolf, S. H.; Celia, M. A.; Hess, K. M. Evaluation of hydraulic conductivities calculated from multiport-permeameter measurements. *Ground Water* **1991**, *29* (4), 516−525.

(32) Garabedian, S. P.; Gelhar, L. W.; Celia, M. A. *Large-Scale Dispersive Transport in Aquifers: Field Experiments and Reactive Transport Theory.;* MIT Parsons Lab Report 315. **1988**.

(33) MirallesWilhelm, F.; Gelhar, L. W. Stochastic analysis of sorption macrokinetics in heterogeneous aquifers. *Water Resour. Res.* **1996**, *32* (6), 1541−1549.

(34) Ren, J. H.; Packman, A. I.; Welty, C. Correlation of colloid collision efficiency with hydraulic conductivity of silica sands. *Water Resour. Res.* **2000**, *36* (9), 2493−2500.

(35) Dong, H. L.; Onstott, T. C.; DeFlaun, M. F.; Fuller, M. E.; Scheibe, T. D.; Streger, S. H.; Rothmel, R. K.; Mailloux, B. J. Relative dominance of physical versus chemical effects on the transport of adhesion-deficient bacteria in intact cores from South Oyster, Virginia. *Environ. Sci. Technol.* **2002**, *36* (5), 891−900.

(36) Mailloux, B. J.; Fuller, M. E.; Onstott, T.; Tullis, C.; James, H.; Dong, H.; DeFlaun, M. F.; Streger, S. H.; Rothmel, R. K.; Green, M.; Swift, D. J. P.; Radke, J. The role of physical, chemical, and microbial heterogeneity on the field-scale transport and attachment of bacteria. *Water Resour. Res.* **2003**, *39* (6) SBH 2−1.

(37) Maxwell, R. M.; Kastenberg, W. E. Stochastic environmental risk analysis: an integrated methodology for predicting cancer risk from contaminated groundwater. *Stochastic Environ. Res. Risk Assess.* **1999**, *13* (1−2), 27−47.

(38) Kinzelbach, W. The Random Walk Method in Pollutant Transport Simulation. In *Groundwater Flow and Quality Modeling*; Custido, A. G. E., Ferreria J. P. L., Eds.; D. Reidel: Norwell, MA, 1988; pp 227−246.

(39) LaBolle, E. M.; Fogg, G. E.; Tompson, A. F. B. Random-walk simulation of transport in heterogeneous porous media: Local mass-conservation problem and implementation methods. *Water Resour. Res.* **1996**, *32* (3), 583−593.

(40) Tompson, A. F. B.; Gelhar, L. W. Numerical-simulation of solute transport in 3-dimensional, randomly heterogeneous porous-media. *Water Resour. Res.* **1990**, *26* (10), 2541−2562.

(41) Valocchi, A. J.; Quinodoz, H. A. M. Application of the Randomwalk Method to Simulate the Transport of Kinetically Adsorbing Solutes. In *Third IAHS Scientific Assembly*, No. 185; IAHS Publishers: Wallingford, UK, **1989**; pp 35−42.

(42) Michalak, A. M.; Kitanidis, P. K. Macroscopic behavior and random-walk particle tracking of kinetically sorbing solutes. *Water Resour. Res.* **2000**, *36* (8), 2133−2146.

(43) Liu, H. H.; Bodvarsson, G. S.; Pan, L. Determination of particle transfer in random walk particle methods for fractured porous media. *Water Resour. Res.* **2000**, *36* (3), 707−713.

(44) Zhang, P. F.; Johnson, W. P.; Scheibe, T. D.; Choi, K.-H.; Dobbs, F. C.; Mailloux, B. J. Extended tailing of bacteria following breakthrough at the Narrow Channel focus area, Oyster, Virginia. *Water Resour. Res.* **2001**, *37* (11), 2687−2698.

(45) Scheibe, T. D.; Wood, B. D. A particle-based model of size or anion exclusion with application to microbial transport in porous media. *Water Resour. Res.* **2003**, *39* (4), 3-1−3-10.

(46) Tompson, A. F. B.; Dougherty, D. E. Particle-grid methods for reacting flows in porous-media with application to Fisher Equation. *Appl. Math. Modell.* **1992**, *16* (7), 374−383.

(47) Tompson, A. F. B.; Ababou, R.; Gelhar, L. W. Implementation of the 3-dimensional turning bands random field generator. *Water Resour. Res.* **1989**, *25* (10), 2227−2243.

(48) Ashby, S. F.; Falgout, R. D. A parallel multigrid preconditioned conjugate gradient algorithm for groundwater flow simulations. *Nucl. Sci. Eng.* **1996**, *124* (1), 145−159.

(49) Jones, J. E.; Woodward, C. S. Newton-Krylov-multigrid solvers for large-scale, highly heterogeneous, variably saturated flow problems. *Adv. Water Resour.* **2001**, *24* (7), 763−774.

(50) Kollet, S. J.; Maxwell, R. M. Integrated surface-groundwater flow modeling: A free-surface overland flow boundary condition in a parallel groundwater flow model. *Adv. Water Resour.* **2006**, *29* (7), 945−958.

(51) Doherty, J. *PEST: Model-Independent Parameter Estimation, User Manual, Version 5*; Watermark Numer. Comput.: Brisbane, Australia, **2004**.

(52) Mutsvangwa, C.; Mutaurwa, B.; Mazhandu, M.; Kubare, M. Application of Harvey-Garabedian model for describing bacterial removal in sand abstraction systems associated with ephemeral rivers. *J. Contam. Hydrol.* **2006**, *88* (1−2), 55−68.

(53) Anderson, M. P. *Characterization of Geological Heterogeneity*. In *Subsurface Flow and Transport: A Stochastic Approach*; G.D.a.S.P. Neuman, Ed.; Cambridge University Press/ UNESCO: Cambridge, UK, 1997.

(54) Zhu, J. F.; Yeh, T. C. J. Characterization of aquifer heterogeneity using transient hydraulic tomography. *Water Resour. Res.* **2005**, *41* (7), W07028.

(55) Harvey, R. W.; Metge, D. W.; Kinner, N.; Mayberry, N. Physiological considerations in applying laboratory-determined buoyant densities to predictions of bacterial and protozoan transport in groundwater: Results of in-situ and laboratory tests. *Environ. Sci. Technol.* **1997**, *31* (1), 289−295.

Received for review November 10, 2006. Revised manuscript received April 20, 2007. Accepted May 17, 2007.

ES062693A